R E V I E W

Investigation of structural and electronic properties of epitaxial graphene on 3C–SiC(100)/Si(100) substrates

Noelle Gogneau[1]
Amira Ben Gouider Trabelsi[2]
Mathieu G Silly[3]
Mohamed Ridene[1]
Marc Portail[4]
Adrien Michon[4]
Mehrezi Oueslati[2]
Rachid Belkhou[3]
Fausto Sirotti[3]
Abdelkarim Ouerghi[1]

[1]Laboratoire de Photonique et de Nanostructures, Centre National de la Recherche Scientifique, Marcoussis, France; [2]Unité des Nanomatériaux et Photonique, Faculté des Sciences de Tunis, Université de Tunis El Manar Campus Universitaire, Tunis, Tunisia; [3]Synchrotron-SOLEIL, Saint-Aubin, BP48, F91192 Gif sur Yvette Cedex, France; [4]Centre de Recherche sur l'HétéroEpitaxie et Ses Application, Centre National de la Recherche Scientifique, Valbonne, France

Correspondence: Noelle Gogneau
Laboratoire de Photonique et de Nanostructures, Centre National de la Recherche Scientifique, Route de Nozay, Marcoussis, 91460, France
Email noelle.gogneau@lpn.cnrs.fr

Abstract: Graphene has been intensively studied in recent years in order to take advantage of its unique properties. Its synthesis on SiC substrates by solid-state graphitization appears a suitable option for graphene-based electronics. However, before developing devices based on epitaxial graphene, it is desirable to understand and finely control the synthesis of material with the most promising properties. To achieve these prerequisites, many studies are being conducted on various SiC substrates. Here, we review 3C–SiC(100) epilayers grown by chemical vapor deposition on Si(100) substrates for producing graphene by solid state graphitization under ultrahigh-vacuum conditions. Based on various characterization techniques, the structural and electrical properties of epitaxial graphene layer grown on 3C–SiC(100)/Si(100) are discussed. We establish that epitaxial graphene presents properties similar to those obtained using hexagonal SiC substrates, with the advantage of being compatible with current Si-processing technology.

Keywords: epitaxial graphene, electronic properties, structural properties, silicon carbide

Introduction

Graphene is a new class of material that is intensively studied, which points to its remarkable physical properties. Today, graphene is presented as a promising material for the observation of novel quantum phenomena and for the development of next-generation electronic and photonic nanodevices.[1,2] Recent applications, such as in photodetectors, transparent electrodes, or energy storage, have established the large capacities of this material. A high-mobility graphene field-effect transistor (FET) array was fabricated on a flexible substrate using Al_2O_3 or h-BN as a gate dielectric in a self-aligned device configuration.[3]

Graphene is an allotrope of carbon that is a single sheet of sp^2-bonded carbon atoms densely packed in a honeycomb crystal lattice. Several promising methods have been reported on the synthesis of graphene. Therefore, micromechanical and chemical exfoliation of graphite,[4–7] thermal chemical vapor deposition (CVD) growth on transition-metal substrates,[8–14] CVD growth on semiconductors,[15] plasma-enhanced CVD,[16–19] graphite oxide reduction,[5,20–22] and thermal decomposition on silicon carbide (SiC) substrates[23,24] have been investigated. While exfoliated graphene flakes are considered the purest graphene with the highest recorded mobility, the limited size of the flakes prevents their use in commercial devices. The approach associating the chemical and thermal reduction of graphene oxide appears as promising. However, graphene sheets present structural defects, which may affect the mechanical and electrical properties. In addition, they tend to form irreversible agglomerates that are damageable, as their unique properties are only associated with individual sheets. With regard to CVD

procedures based on metal substrates, although good quality and large areas of graphene can be achieved, graphene sheets need to be transferred onto insulating substrates for device applications. Nevertheless, this transfer step, using an invasive chemical treatment, is inevitably damaging to graphene-sheet properties.

The epitaxial graphene (EG) layer on single-crystalline SiC substrates is considered the most promising technology for graphene-based electronics. In fact, the graphene synthesis following this procedure shows electronic properties similar to isolated graphene sheets. In addition, for the semiconductor industry, this approach also presents the advantage of obtaining graphene directly on an insulating substrate (SiC), and thus does not require any transfer before processing devices.

Recently, the EG layer was largely synthesized and the intrinsic mechanisms of EG were highlighted on hexagonal SiC bulk substrates.[23,25,26] Economically, however, the rather-high price of bulk hexagonal SiC substrates and their limited size are an obstacle for large-scale fabrication of graphene devices. To solve this crucial drawback, synthesis of the EG layer on a thin crystalline SiC layer formed on silicone substrates has been studied.[27–30] This graphene-on-silicon method enables the formation of a large layer of well-ordered sp^2 carbon networks on Si substrates and to fabricate electronic devices.[31] Therefore, graphene synthesis on Si(111) can be used to form a channel for digital field-effect transistor operation at the terahertz frequency,[27] while graphene on Si(110) and Si(100) can be used for ultrahigh-speed optical communications.[32,33] Among different applications, biomedical applications of graphene have attracted increasing interest over the last few years.[1] Among studies performed on graphene for biomedical applications, a lot of interesting studies have been carried out to explore the use of graphene as an antibacterial material, for biological sensing and imaging, and as a biocompatible scaffold for cell culture.[34]

Numerous studies on the structural and electrical properties of graphene synthesized on a crystalline 3C–SiC(111)/Si(111),[35–41] 3C–SiC(111)/Si(110),[29] and 3C–SiC(111)/Si(100) substrates have been reported.[38,42–44] It has been established that the graphitization process on SiC(111)/Si(111) is similar to that on the Si-terminated SiC bulk substrates with the presence of a buffer layer at the graphene–SiC(111) interface. In contrast, graphene formed on SiC(111)/Si(110) is characterized by the absence of a buffer layer.[42,44] The fabrication of an EG layer on a 3C–SiC(100)/ Si(100) wafer with the most promising properties is very challenging, since it requires the formation of high-quality, large, and homogeneous single and bilayers of graphene. Although attempts to grow EG on this epilayer substrate have been reported,[5,38] this silicon-substrate orientation for graphene epitaxy remains under investigation. In this paper, our work dealing with the structural and electronic properties of EG layers grown on 3C–SiC(100)/Si(100) epilayers by solid-state graphitization in an ultrahigh vacuum (UHV) is reviewed.

Experimental details

The substrates consist of 3C–SiC epilayers grown on Si(100) substrates by CVD. Deposition occurs within a resistivity-heated hot-wall reactor using silane and propane gases as precursors diluted in hydrogen. After a carbonization step performed at 1,100°C, leading to the formation of an SiC nucleation layer by the reaction of propane with the Si substrate, a 1,500 nm-thick SiC is grown by exposing the surface to propane and silane precursors diluted in hydrogen (~0.01%–0.02%) at 1,350°C and at a reactor pressure of 200 mbar. The surface of these heteroepitaxial materials is characterized by antiphase domain (APD) boundaries. More details about the 3C–SiC growth method can be found in Portail et al.[45]

Graphene layers are prepared in a UHV by electron-bombardment heating of 3C–SiC(100)/Si(100) substrates. Prior to graphene formation, the pseudosubstrates are first outgassed for several hours at 600°C under UHV conditions and then annealed at 900°C under a silicon flux (2 Å/minute) to remove the surface-contamination layer and the native oxide. Afterward, the temperature is increased between 1,150°C and 1,300°C for a few minutes in order to achieve surface graphitization. During this procedure, the substrate temperature is monitored with an infrared pyrometer, and the base pressure of the system is maintained at around 2.1^{-10} Torr, with a peak pressure of 10^{-9} Torr during the graphitization process. This method to form EG on a 3C–SiC(100)/ Si(100) epilayer surface is similar to the one used on the 3C–SiC(111) pseudosubstrate.[37]

Graphene samples are further cooled to room temperature and transferred ex situ for characterization. By combining micro-low-energy electron diffraction (μ-LEED), low-energy electron microscopy (LEEM), atomic force microscopy (AFM), Raman spectroscopy, and surface-potential (SP) and X-ray photoelectron spectroscopy (XPS), the structural and electrical properties of the EG layer grown on the 3C–SiC(100) pseudosubstrate are determined.

Structural properties of epitaxial graphene on 3C–SiC(100)/Si(100): results and discussion

The graphitization of the SiC surface is achieved by solid-state graphitization. It consists of Si sublimation from the SiC surface, enabling carbon enrichment of the surface.[23,46] This graphitization step is monitored by LEED. The LEED pattern is collected to investigate the structural properties and the graphitization process of the sample surface. Initially, during the annealing of the sample under Si flux at 900°C, the LEED pattern is characterized by Si-rich (3×2) and (2×1) surface reconstruction. Transition from the Si- to the C-rich surface due to the sublimation of Si-0surface atoms takes place in the 1,050°C–1,100°C temperature range, and the c(2×2) reconstruction begins to develop during annealing between 1,100°C and 1,150°C. This phase is usually interpreted as a C-terminated structure.[47] Further annealing induces the coexistence of the graphene layers and the (2×1) surface reconstruction of 3C–SiC(100). Finally, under UHV conditions, annealing at a minimum temperature of 1,150°C is required to develop the (1×1) graphitic phase on the SiC pseudosubstrate.

Typical diffraction patterns of 2-monolayer (ML)-thick graphene layers synthesized by annealing sample at 1,150°C during 10 min are shown in Figure 1A. Two contributions can be clearly distinguished. The first contribution corresponds to the (2×1) cubic surface of the 3C–SiC(100) epilayer (white boxes), while the second is due to the two-domain hexagonal (1×1) graphene layer, confirming the presence of the graphene layer on the 3C–SiC(100)/Si(100) (white and blue arrows). This double contribution can be understood as the result of any of the following two phenomena: 1) a graphene domain oriented with +15° to the [110] direction of the inphase/anti-phase 3C–SiC(100) domains will appear at ±15° in the LEED images (Figure 1B); and 2) a possible alternative consists in the presence of two hexagonal lattices rotated by ±15° with respect to a single-domain square SiC lattice (Figure 1C).

If we analyze finely the second contribution establishing the presence of EG on the surface, we observe that two sets of spots are present in reciprocal space. Other than the rotation by ±15° outlined earlier, an additional ±2° misalignment can be observed, indicated by the double white arrows on the magnification of Figure 1A. This rotation is assigned to the misalignment between the first layer and the second graphene layer constituting the analyzed sample.[48] Therefore, by considering the double contribution and the misalignment of the graphene contribution evidenced
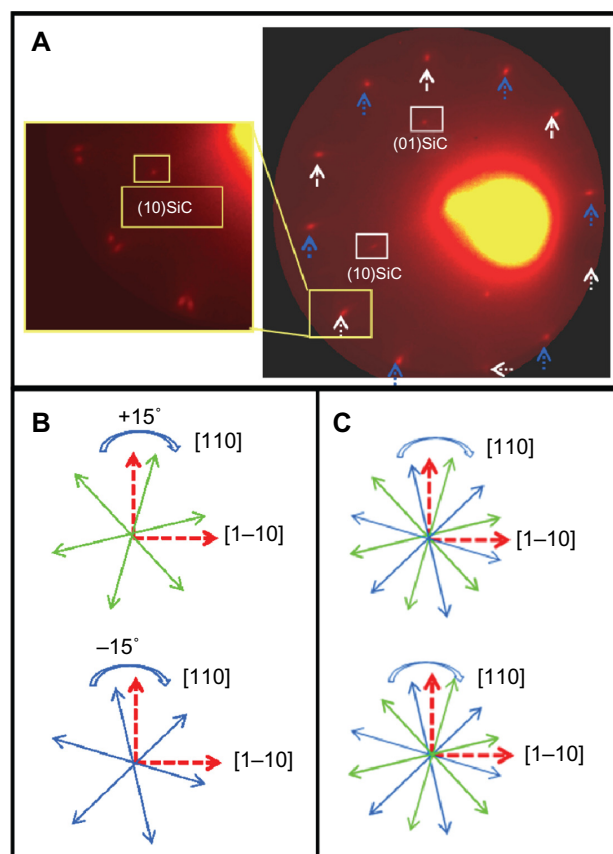

Figure 1 (**A**) μ-Low-energy electron diffraction (LEED) images (Ep =46 eV) of epitaxial graphene (1.5 layers) on 3C–SiC(100) taken on different regions. The intense bright large spot is due to backscattered secondary electrons. The magnification shows the two sets of spots present in reciprocal space, corresponding to the misalignment between the graphene layer. (**B** and **C**) Crystallographic axes of the graphene layer and cubic substrates determined from the LEED images.

by the LEED image, we can conclude that the graphene layer consists mainly of two hexagonal lattices rotated by ±15° (±2°) with respect to the square 3C–SiC lattice. This would be in agreement with the recent scanning tunneling microscopy observations of Chaika et al[49] consisting of two domains rotated by ±13.5° from the (110) axis and two domains rotated by ±13.5° from the (1–10) axis, which generates 24 LEED spots.

The graphene layer is further studied by LEEM in order to evaluate thickness spatial distribution.[50,51] During the LEEM experiments (LEEM III; Elmitec, Clausthal-Zellerfeld, Germany), the electron gun and sample are biased at 20 kV. The bright-field (BF) and dark-field (DF) LEEM images (Figure 2) have been obtained by selecting the corresponding LEED spots via an aperture (contrast aperture) placed on the optical path of the microscope column.

A typical BF LEEM pattern from an EG layer achieved for electron energy of 2.69 eV is represented in Figure 2A.
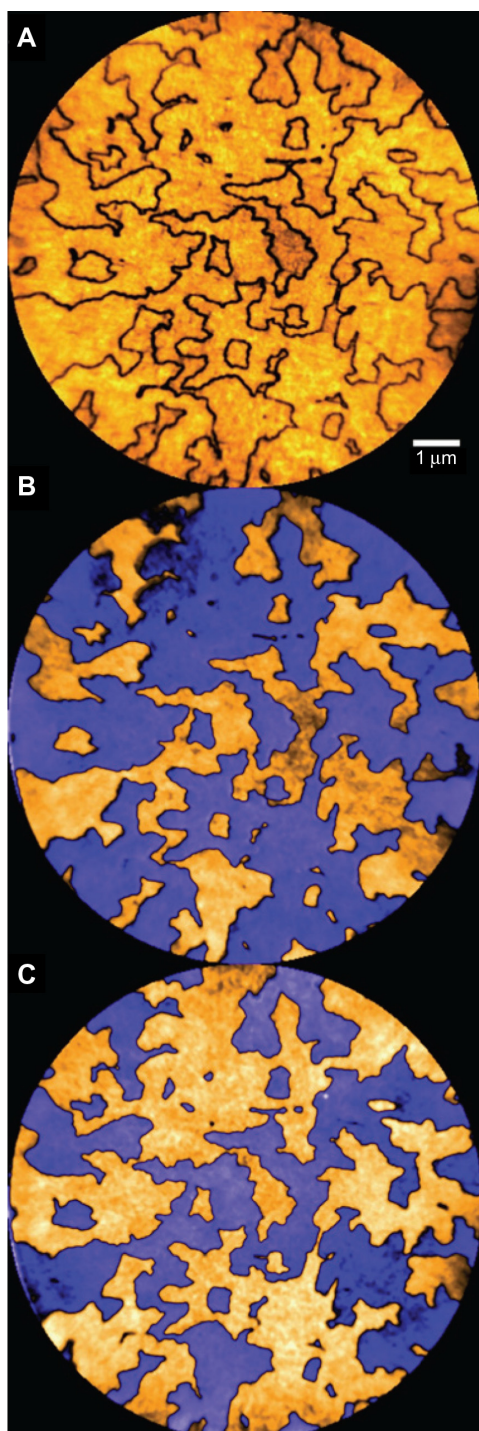
Figure 2 Low-energy electron microscopy images of sample covered by 1.5 layer of graphene.
Notes: (**A**) Bright-field image (VST [start voltages] =2.69 eV); (**B**) dark-field image (VST =7.97 eV) for the (01)SiC low-energy electron diffraction (LEED) spot; (**C**) dark-field image (VST =7.97 eV) for the (10)SiC LEED spot. The field of view is 25 μm.

In different regions, the image-intensity levels change in different manners. The layer exhibits large domains separated by thin black lines. These fine structures can be caused by the thickness in homogeneity (mono/bilayer graphene) over the surface, this mono/bilayer distribution

being characterized by two hexagonal lattices rotated by ±15° with respect to the square SiC lattice.

Figure 2B and C present DF LEEM images from the two SiC LEED spots "(01)SiC" and "(10)SiC" represented on the LEED pattern from Figure 1A. Depending on which LEED spot is considered, the intensity on the LEEM images is reversed. This result indicates that the domains of 3C–SiC(100) on Si(100) have twofold symmetry. Due to the alternating layer-stacking sequence in the [001] crystallographic direction of 3C–SiC(100), the substrate surface possesses only a twofold symmetry, which would necessarily imply that only one of the domains should be present. The presence of both domains indicates that the 3C–SiC layer presents two distinct epitaxial orientations with respect to the Si(100) substrate: [100]//[100] or [100]//[010].[41] Comparison of the BF LEEM image with the two DF LEEM images clearly indicates that the black lines between the large domains of graphene layers can be correlated with the domain boundaries of the 3C–SiC(100). We thus establish that the graphene areas are delimited by the domains of the substrate.

At this stage, one may wonder what the factors limiting the size of graphene domains are. Before graphitization, the SiC(100)/Si(100) surface is characterized by APD with stepped terraces (Figure 3A).[41] After graphitization, within a given APD, the graphene layer is constituted by atomically flat terraces, as evidenced by AFM imaging (Figure 3). This observation establishes that the graphene layers are not limited by the SiC terraces, but rather by their surface symmetry, and the APDs initially characterizing the 3C–SiC(100) surface. This result shows that graphitization achieved by Si sublimation from the SiC surface is strongly affected by the substrate morphology.

Synthesis of material with the most promising properties requires the formation of mono- and bilayer graphene with controllable characteristics, dimensions, and localization. It is known that graphitization begins from the step edge and progresses towards the terraces. The EG layers are formed during the early stages of thermal desorption of Si from the SiC surface. However, this does not necessary lead to a uniformly graphitized surface. Important parameters governing the formation of graphene by solid-state graphitization from the SiC surface are the annealing temperature at which the sublimation of Si atoms occurs and the duration of this annealing. In order to control the degree of graphitization, the evolution of surface graphitization was investigated as a function of synthesis temperature for a graphitization duration of 10 minutes. Then, three different samples
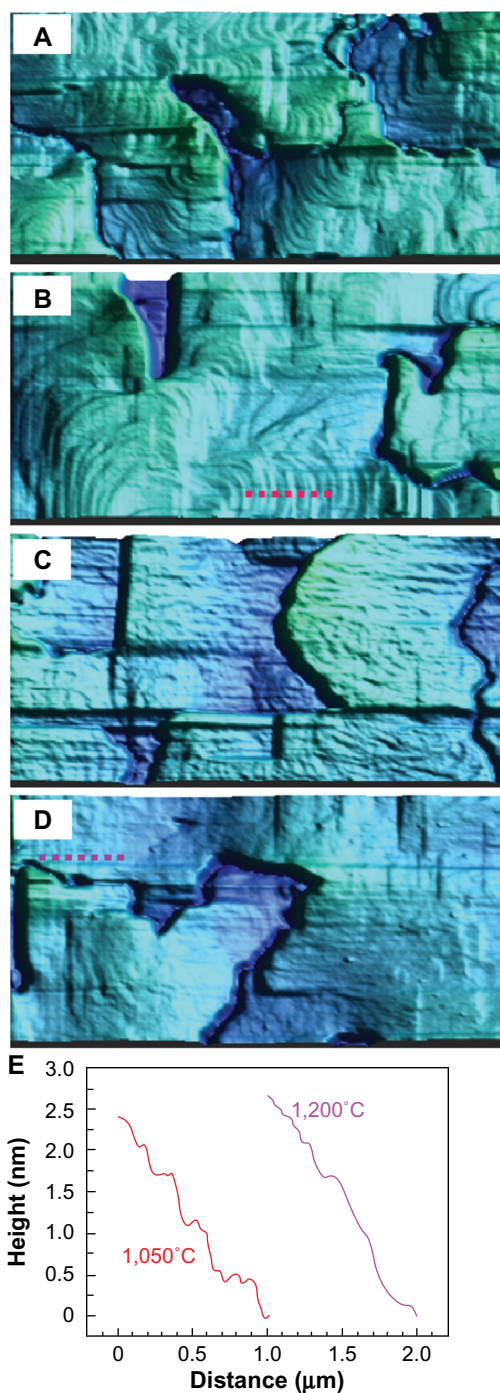
Figure 3 3-D-flattened atomic force microscopy images (5×2.5 μm) of the 3C–SiC(100)/Si(100) surface before (**A**) and after annealing at 1,050°C (**B**), 1,150°C (**C**), and 1,200°C (**D**). (**E**) Step profile performed on samples S1 (red curve) and S3 (purple curve) indicated by the dashed lines in (**B** and **D**).

(S1, S2, and S3) were analyzed, heated at 1,050°C, 1,150°C, and 1,200°C, respectively. The surface morphology at a microscopic scale of the 3C–SiC(100) surface was studied by AFM. The AFM imaging technique, performed in tapping mode with an Al-coated tip characterized by a tip radius of 7 nm, is an efficient technique in ambient conditions that

enables rapid and convenient characterization of the surface. Figure 3 presents a series of 3-D topographic images of the semi-insulating 3C–SiC(100)/Si(100) surface before and after graphitization.

The surface of as-grown 3C–SiC heteroepitaxial substrates without any heat treatment is characterized by APD boundaries presenting stepped surfaces (Figure 3A). The sample heated at 1,050°C (S1) still shows domains, always delimited by APD. These domains present well-defined steps through energy minimization, resulting in a reconstructed surface (Figure 3B). This surface feature shows that sublimation of Si atoms leading to graphene formation does not occur in these growth conditions at 1,050°C. By contrast, smoother domains, with the surface appearing flatter as if covered with a continuous layer, characterized samples heated at higher temperatures, 1,150°C for sample S2 (Figure 3C) and 1,200°C for sample S3 (Figure 3D).

Interestingly, the continuity of the graphene layer observed here is in accord with results obtained for the growth of graphene layers on 6H–SiC vicinal substrates, where a carpet-like growth mode covering several substrate terraces and steps is observed by scanning tunneling microscopy and AFM images.[26,52] This behavior is confirmed by comparing the step profile of samples S1 and S3 (Figure 3E). This specific variation of surface morphology with temperature is the clear signature of graphene formation.[35] The results displayed previously reveal that the sublimation of few atomic layers of Si out of the SiC epilayer starts by annealing of the surface at 1,150°C or higher. In these used conditions and depending on the temperature and duration of graphitization, the surface is covered by single or multiple layers of graphene. Graphitization of the 3C–SiC(100) surface leads to a remarkable modification of the surface morphology on a microscopic scale. These results indicate the possibility of controlling the growth of large-scale graphene on 3C–SiC(100) beyond the SiC terraces. However, before developing devices based on few-layers EG, the thickness as well as the uniformity of the graphene coverage must be controlled.

Raman spectroscopy is the technique of choice to access graphene-layer thickness and uniformity. Micro-Raman spectroscopy was performed at room temperature with a Jobin Yvon T64000 (Horiba, Kyoto, Japan) spectrometer in a backscattering confocal configuration. The excitation source was an Ar+ laser at a wavelength of 488 nm, and laser power was controlled at 5 mW on the sample surface. We used a 100× objective lens for focusing the laser beam on the surface and collecting the scattered light at room-temperature measurements from different local spots forming

a pixel pattern. The spatial resolution of the image was 1 μm, while the spectral resolution was less than 0.35 cm⁻¹.

Figure 4A represents a typical Raman spectrum obtained in the frequency range (1,000–3,000 cm⁻¹). We observed the most prominent Raman features: D, G, 2D, and G', characterizing graphene (see Table 1). The G band corresponds to the doubly degenerate (transverse optical and longitudinal optical) phonon mode associated with E_{2g} symmetry at the Brillouin zone center (the Γ-point), which gives evidence of carbon sp² reorganization.[53,54] Its peculiar position value (1,594 cm⁻¹) indicates the existence of a strong level of doping and a compressive stress of the layer.[55] The D band, at 1,372 cm⁻¹, involves phonons near the K-points normally absent in defect-less graphene.[56] Its presence is the signature of structural disorder, including corrugation and distortions attributed to twisting, and step edges, such as finite-size domains, atomic-scale defects, and armchair-type edge defects.[57–59] The G' band corresponds to an intervalley process involving one transverse optical and one longitudinal optical phonon at the K-point.[60,61] Finally, the 2D band is assigned to the second order of the

D band, where it is associated with two phonons close to the K-point in the Brillouin zone.[62] The (D + G) peak corresponds to 2LO (K) activated by disorder due to the presence of defects in the graphene layers.

Intensity mapping is performed over a surface of (300×300 μm²) in regular locations along *x* and *y* directions across the sample surface to ensure that all changes in graphene modes will be detected. The local mapping intensity of the G and 2D bands showed great similarity in graphene distribution across the sample surface (see Figure 5A and B).

We observed black flakes nonuniformly distributed across the sample surface surrounded by a more brightly colored area corresponding to maximum graphene-layer numbers. The layer number was identified by investigating the intensity ratio of the G and 2D bands (I_G/I_{2D}). The false color cartography in Figure 5C represents the intensity ratios of the G and 2D bands. Seventy percent of the surface exhibits an intensity ratio I_G/I_{2D} centered on 1.2, which indicates multilayer-graphene covering of the sample surface (3 layer graphene).[63–66]

From the intensity ratio of the D and G bands, we evaluated the domain size (L_a) of the graphene layer given by the following expression:[67,68]

$$L_a(nm) = \frac{560}{E_{laser}^4}\left(\frac{I_D}{I_G}\right)^{-1}, \qquad (1)$$

where $I_D(I_G)$ is the intensity of the D (G) Raman mode and E_{laser} the excitation-laser energy ($E_{laser} = 2.54\ eV$). L_a of EG layers grown on 3C–SiC (100) epilayer is about 17.8 nm. The smaller domain size, normally absent for highly smooth EG, could be assigned to the pseudosubstrate-morphology effect. In fact, a possibility of Bernal stacking of EG similar to exfoliated graphene has been reported.[69] This possible effect can be investigated by performing polarized Raman spectroscopy measurement.

The polarization behavior of graphene Raman modes is presented in Figure 4B and C. Backscattering geometry $(Z[x, -]\bar{Z})$, where the incident laser-beam polarization is fixed in the *x* direction and the polarization of the scattered light by the sample is selected in $(Z[x, x]\bar{Z})$ parallel (p-polarization) or $(Z[x, y]\bar{Z})$ perpendicular (s-polarization) configurations, was used. Within this approach, graphene surface-roughness dependence is investigated by analyzing the (I_D/I_G) intensity-ratio variation in both configurations. The intensity ratio (I_D/I_G) reaches high intensity in s-polarization (cf Table 1), reflecting the Raman graphene modes, since the relative intensities of each showed a particular behavior.
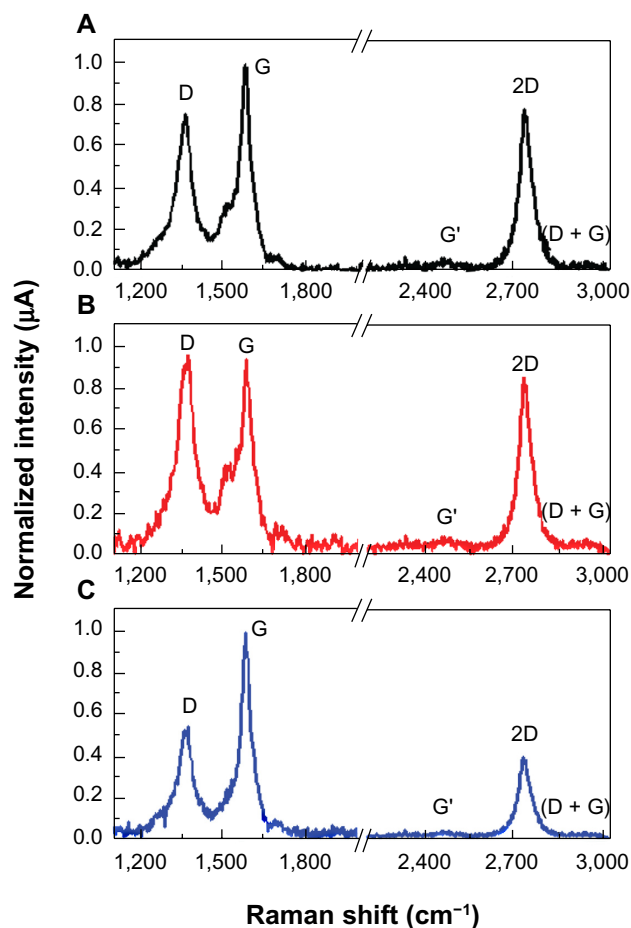

Figure 4 Raman spectra of graphene layers grown on 3C–SiC(100) on Si(100) substrate.
Note: (**A**) unpolarized, (**B**) in p-polarization, (**C**) in s-polarization.

Table I Raman shift of the graphene modes grown on 3C–SiC(100)/Si(100) substrate

Raman modes and ratio	D (cm⁻¹)	G (cm⁻¹)	G' (cm⁻¹)	2D (cm⁻¹)	D + G (cm⁻¹)	I_G/I_{2D}	I_D/I_G unpolarized	I_D/I_G (s)	I_D/I_G (p)
Raman shift and ratio	1,372	1,593	2,467	2,733	2,948	1.2	0.75	1.02	0.53

The G band belongs to the D_{3h} space group ($P\bar{6}m2$) in the (Γ) point for three-layer graphene in AB stacking. The associated irreducible representation is given by the following expression:[60]
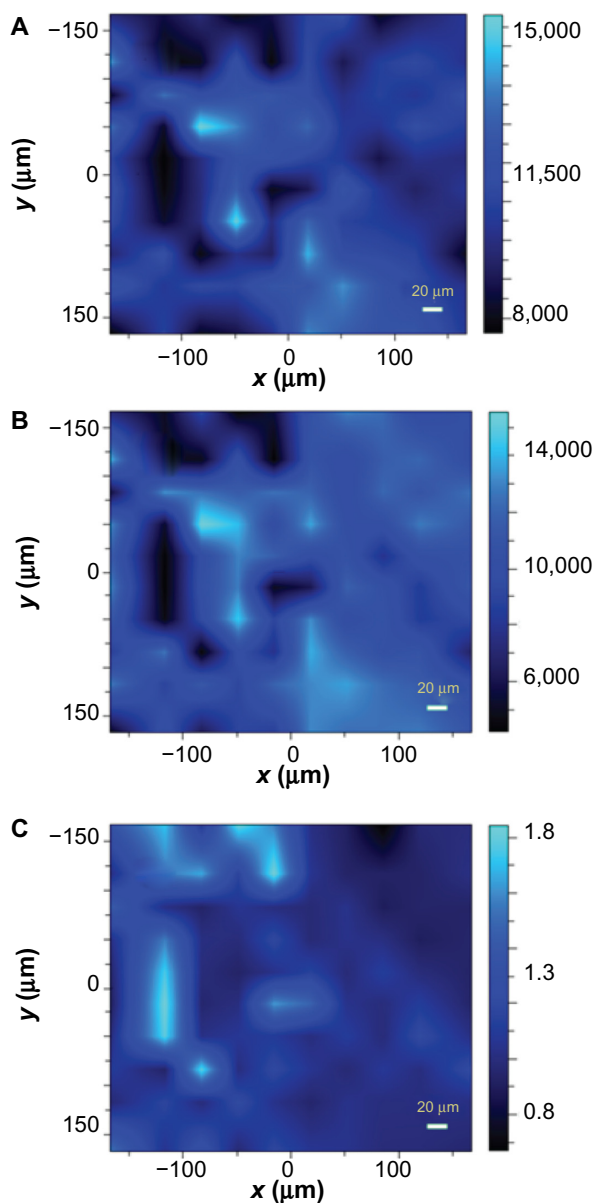
$$\Gamma^{Raman} = 3E' + 2\,(E'' + A_1'), \qquad (2)$$

the G band being assigned to a combination of E' and E'' representations, and also the A_1' representation is Raman-active with a lower-frequency component and its mode has no polarization dependence (Figure 4), which makes it permitted in p- and s-configurations.[55,70] With regard to the D peak (,) which is assigned to the breathing mode involving phonons near the K-zone boundary, its intensity is not affected by the layer number, whereas its mode shows a high dependence on the amount of disorder.[71] This disorder can result from the graphene layer and/or from the angle between the incident polarizations and the graphene-flake edge.

Whatever the edge orientation and disorder, D intensity reaches the maximum for polarization parallel to the edge and the minimum when polarization is perpendicular to the edge, without reaching zero for light polarized perpendicular to the edge.[71] The maximum intensity of the D band for parallel configuration proves that the graphene flake is parallel to the average edge direction, and the decrease of the D-band intensity in s-polarization indicates that the degree of disorder is not homogeneous in the two directions of the graphene layer and the grains are dissymmetric.[71] This defect variation could be related to the roughness of the substrate. However, investigation of the change of the growth axes of 3C–SiC(100) on the off-axis Si(100) substrate that could originate from the thermal effect occurring during the graphitization process has demonstrated that non-Bernal stacking can be related to pseudosubstrate morphology.[72] By consequence, a domain size of the order of 17.8 nm cannot be assigned to the surface morphology of the substrate, but to the intrinsic formation of the hexagonal phase on the cubic folder symmetric surface, due to the presence of different interdistances between defects in the EG layer.[59]

Based on the structural properties discussed in this review, it is interesting to underline that the growth of graphene, and specifically of the first graphene layer on 3C–SiC(100)/Si(100) substrate, is similar to that reported for the carbon-terminated 6H–SiC substrates. Surface coverage with single or multiple layers of graphene can be adjusted by modulating the graphitization parameters (temperature and duration), and the carbon enrichment of the surface is characterized by a specific surface structure. The specificity of EG layers grown on 3C–SiC(100)/Si(100) resides in the fact that graphene

Figure 5 Mapping Raman intensity of G band (**A**), 2D band (**B**), and the ratio of the G band on the 2D band, ie, I_G/I_{2D} ratio (**C**) of graphene grown on 3C–SiC(100)/Si(100) substrate.

layers do not present a rotational disorder, in contrast to previous observations of few-layers graphene on SiC(000-1) substrate, which exhibits a high degree of disorder.[38]

Electrical properties of epitaxial graphene on 3C–SiC(100)/Si(100): results and discussion

One of the major challenges for EG-grown films is to understand the influence of graphitization conditions not only on the film structure but also on the electrical properties. The substrate, in addition to influencing the growth mechanism during synthesis, can significantly influence the electrical properties. In fact, according to the substrate nature, the degree of graphitization may be different for the same synthesis conditions. However, EG coverage affects the electrical properties of graphene.

In order to establish the graphene thickness–electrical properties relation, SP measurements can be performed. The SP mode, also called the Kelvin mode, is an AFM technique offering a powerful tool for measuring the distribution of the electric potential of a surface with nanometer resolution. This technique creates the SP image by detecting the interactions between the conductive tip and the sample through long-range Coulomb forces. SP mapping of the surface was achieved with a Cr/Pt-coated tip characterized by a tip radius of 10 nm and with a lift-scan height of 20 nm (lift mode). Figure 6A–C present SP images performed in the same conditions on three different surfaces: the c(2×2)-3C–SiC(100) reconstructed, ie, sample annealed but not covered by the graphene layer, and two different stages of the EG-layer formation, corresponding to the sample covered by 1.5 ML and 2.8 ML of graphene. The SP profiles corresponding to the maps through the x-axis are shown in Figure 6D. The average SP extracted from these profiles as a function of the EG coverage are plotted on Figure 6E, with the error bar corresponding to the peak-to-valley value.

The SP, significant for each material, is related to the work function required to move an electron from the material to the vacuum. It can be defined as:

$$e \cdot SP^{measured} = W_{tip} - W_{sample}, \qquad (3)$$

where W_{tip} and W_{sample} are the work functions of the tip and the graphene-sample surface, respectively, and e is the elementary charge.[73,74] While W_{tip} is unknown, because the same tip with the same imaging conditions have been used to analyze all samples, W_{tip} remains constant and the different
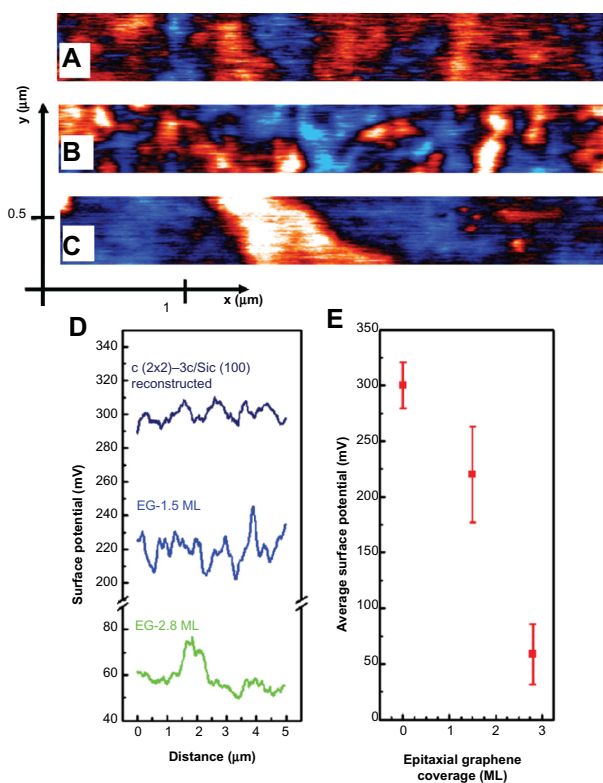

Figure 6 Surface-potential (SP) mapping of (**A**) c(2×2)-3C–SiC(100) reconstructed, ie, sample annealed, but not covered by graphene layer, (**B**) sample covered by 1.5 monolayer (ML) of the epitaxial graphene (EG), and (**C**) sample covered by 2.8 ML of the epitaxial graphene. (**D**) SP profiles through the x-axis corresponding to the SP mapping of (**A–C**). (**E**) Variation of the average SP, extracted from SP profiles as a function of the graphene coverage.

samples may be compared. In these conditions, the variation of the SP reflects the variation of W_{sample}.

The measured SP, plotted in Figure 6, decreases as the EG thickness increases, which demonstrates a corresponding increase of W_{sample} (according to the definition of SP given above). This increase of W_{sample} is in good agreement with results published in the literature.[75–77] In our graphitization conditions, the increase in graphene coverage from 1.5 ML to 2.8 ML corresponds to a decrease of SP of around 161±15 mV, and thus to an increase of W_{sample} by ~160 meV. With layer thickness taken into account, this result is in good agreement with those presented by Filleter et al,[75] who determined that bilayer graphene grown epitaxially on 6H–SiC(0001) increases the work function in the order of 135±9 meV compared to single-layer films.

The thickness of the EG layer strongly influences the electrical properties. However, the nature of the substrate can also influence EG properties; in particular, it can potentially play a crucial role on the formation of a buffer layer. The buffer layer is a graphitic layer covalently bound to the substrate. At this stage, an important question appears: is there an interface layer

between the EG layer and the 3C–SiC(100)/Si(100) epilayer substrate? To answer this question, graphene samples were analyzed by XPS. XPS experiments were performed in UHV conditions on the Tempo beamline at the SOLEIL Synchrotron facility (France). The analyzing chamber was equipped with a Scienta 2000 electron hemispherical analyzer with a delay-line 2D detector (Scienta Scientific, Uppsala, Sweden), which optimized the detection linearity and signal:background ratio. Figure 7 displays C 1s spectra achieved at two different photon energies – 340 eV and 510 eV. A sharp C 1 s peak (blue curve), located at 284.5 eV in binding energy, indicates the presence of sp^2 hybridized C–C bonds. The C 1s spectra showed another component at 283.2 eV in binding energy. These components corresponded to the SiC bulk (green curve).[36,77,78]

It is interesting to note that for a graphene coverage of only 1.5 ML, the bulk SiC signal disappears in the C 1s spectrum collected at a photon energy of 340 eV. This graphene-related component (G) – located at 284.5 eV, ie, shifted by 1.6 eV toward higher binding energy with respect to the bulk SiC – indicates sp^2 hybridized C–C bonds, which are a signature of the graphene layers. At the C 1s core level, the average
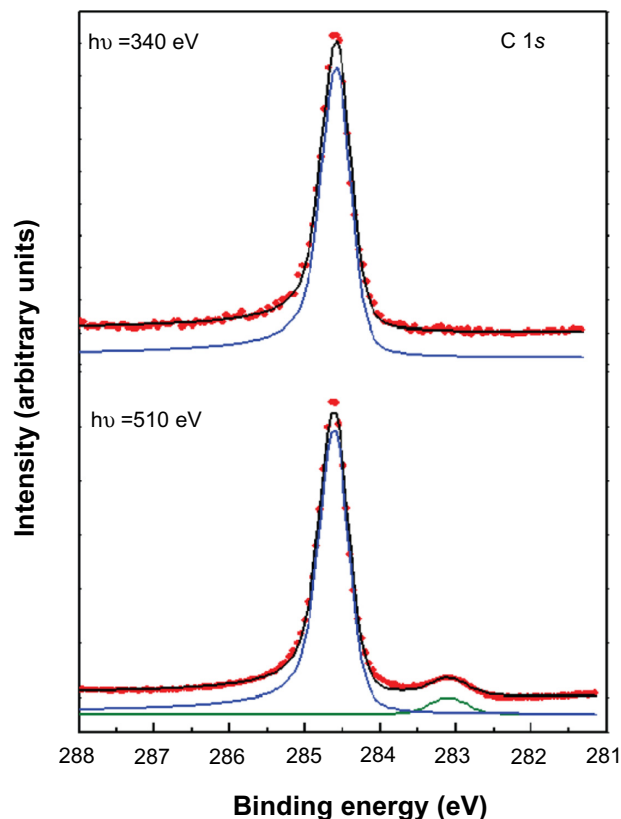
graphene-film thicknesses can be determined by measuring the attenuation of the SiC contribution (282.8 eV) with respect to the graphene signal (284.5 eV).[79] When increasing the incident energy, the line shape and position of the graphene peak remain unaffected. The signature of the bulk SiC substrate appears. By contrast, any third peak, corresponding to the buffer layer present at the graphene–substrate interface, is observed. These results demonstrate the absence of an interfacial graphitic layer covalently bound to 3C–SiC(100).[35,44,80,81] We can conclude that the first graphitic layer grows on 3C–SiC(100) without an interface layer (buffer layer). This result is a major departure with respect to graphene on hexagonal SiC(0001) and graphene on cubic SiC(111),[15,25,36,56] where the first graphene layer, while easy to grow uniformly, is nonconductive. Finally, in the knowledge that the intermediate C-rich layer (buffer layer) degrades the intrinsic mobility of EG layer,[23] its absence is an important property that opens new perspectives for graphene-based electronic devices.

Conclusion

The properties of EG layers discussed in this review evidence the interest in the 3C–SiC(100)/Si(100) pseudosubstrate as a base for graphene synthesis. In fact, the possible control of graphene coverage by controlling the graphitization parameters (temperature and duration) and the absence of an interfacial layer covalently bound to 3C–SiC(100) are important properties that constitute fundamental steps toward the development of Si-based technologies for the mass production of graphene. Although there are many challenges that need to be overcome, such as improvement of the surface morphology of the SiC(100) epilayer characterized by antiphase domain boundaries, which limits the graphene-domain size, this approach will likely open new perspectives for industrial-scale fabrication and mass production. In fact, the EG on SiC/Si(100) substrates presents the advantage of being able to be produced on substrates significantly larger than commercial hexagonal SiC substrates, and of being compatible with current Si-processing techniques, thus offering the opportunity to directly integrate graphene into standard low-cost Si technology.[44] These encouraging and promising results clearly demonstrate that graphene can be an ideal material for future silicon electronic devices. The ability to grow a high-quality graphene layer on silicon substrate will open up new opportunities for semiconductor nanoelectronic technology, making the devices faster, cheaper, and more reliable.

Figure 7 C 1s X-ray photoelectron spectroscopy spectra for epitaxial graphene on 3C–SiC(100)/Si(100) at two different photon energies.
Notes: Blue curve for graphene [C–C], and green curve for Si-C. Red dots are experimental data points. The black curve is the envelope of the fitted components.

Acknowledgments

References

1. Novoselov KS. Nobel lecture: Graphene – materials in the Flatland. *Rev Mod Phys*. 2011;83(3):837–849.
2. Novoselov KS, Falko VI, Colombo L, Gellert PR, Schwab MG, Kim K. A roadmap for graphene. *Nature*. 2012;490(7419):192–200.
3. Lu CC, Lin YC, Yeh CH, Huang JC, Chiu PW. High mobility flexible graphene field-effect transistors with self-healing gate dielectrics. *ACS Nano*. 2012;6(5):4469–4474.
4. Novoselov KS, Geim AK, Morozov SV, et al. Electric field effect in atomically thin carbon films. *Science*. 2004;306(5696):666–669.
5. Stankovich S, Dikin DA, Dommett GH, et al. Graphene-based composite materials. *Nature*. 2006;442(7100):282–286.
6. Blake P, Brimicombe PD, Nair RR, et al. Graphene-based liquid crystal device. *Nano Lett*. 2008;8(6):1704–1708.
7. Hernandez Y, Nicolosi V, Lotya M, et al. High-yield production of graphene by liquid-phase exfoliation of graphite. *Nat Nanotechnol*. 2008;3(9):563–568.
8. Somani PR, Somani SP, Umeno M. Planer nano-graphenes from camphor by CVD. *Chem Phys Lett*. 2006;430(1–3):56–59.
9. Sutter PW, Flege JI, Sutter EA. Epitaxial graphene on ruthenium. *Nat Mater*. 2008;7(5):406–411.
10. Reina A, Jia X, Ho J, et al. Large area, few-layer graphene films on arbitrary substrates by chemical vapor deposition. *Nano Lett*. 2008;9(1): 30–35.
11. Lee Y, Bae S, Jang H, et al. Wafer-scale synthesis and transfer of graphene films. *Nano Lett*. 2010;10(2):490–493.
12. Chae SJ, Güneş F, Kim KK, et al. Synthesis of large-area graphene layers on poly-nickel substrate by chemical vapor deposition: wrinkle formation. *Adv Mater*. 2009;21(22):2328–2333.
13. Li X, Cai W, An J, et al. Large-area synthesis of high-quality and uniform graphene films on copper foils. *Science*. 2009;324(5932):1312–1314.
14. Bhaviripudi S, Jia X, Dresselhaus MS, Kong J. Role of kinetic factors in chemical vapor deposition synthesis of uniform large area graphene using copper catalyst. *Nano Lett*. 2010;10(10):4128–4133.
15. Michon A, Vézian S, Ouerghi A, Zielinski M, Chassagne T, Portail M. Direct growth of few-layer graphene on 6H-SiC and 3C-SiC/ Si via propane chemical vapor deposition. *Appl Phys Lett*. 2010; 97(17):171909.
16. Wang JJ, Zhu MY, Outlaw RA, et al. Free-standing subnanometer graphite sheets. *Appl Phys Lett*. 2004;85(7):1265–1267.
17. Wang J, Zhu M, Outlaw RA, Zhao X, Manos DM, Holloway BC. Synthesis of carbon nanosheets by inductively coupled radio-frequency plasma enhanced chemical vapor deposition. *Carbon*. 2004;42(14): 2867–2872.
18. Malesevic A, Roumen V, Koen S, et al. Synthesis of few-layer graphene via microwave plasma-enhanced chemical vapour deposition. *Nanotechnology*. 2008;19(30):305604.
19. Vitchev R, Malesevic A, Petrov RH, et al. Initial stages of few-layer graphene growth by microwave plasma-enhanced chemical vapour deposition. *Nanotechnology*. 2010;21(9):095602.
20. Verdejo R, Barroso-Bujans F, Rodriguez-Perez MA, Antonio de Saja J, Lopez-Manchado MA. Functionalized graphene sheet filled silicone foam nanocomposites. *J Mater Chem*. 2008;18(19):2221–2226.
21. Schniepp HC, Li JL, McAllister MJ, et al. Functionalized single graphene sheets derived from splitting graphite oxide. *J Phys Chem B*. 2006;110(17):8535–8539.
22. Gilje S, Han S, Wang M, Wang KL, Kaner RB. A chemical route to graphene for device applications. *Nano Lett*. 2007;7(11):3394–3398.
23. Berger C, Song Z, Li X, et al. Electronic confinement and coherence in patterned epitaxial graphene. *Science*. 2006;312(5777): 1191–1196.
24. Berger C, Song Z, Li T, et al. Ultrathin epitaxial graphite: 2D electron gas properties and a route toward graphene-based nanoelectronics. *J Phys Chem B*. 2004;108(52):19912–19916.
25. Emtsev KV, Bostwick A, Horn K, et al. Towards wafer-size graphene layers by atmospheric pressure graphitization of silicon carbide. *Nat Mater*. 2009;8(3):203–207.
26. Seyller T, Emtsev KV, Gao K, et al. Structural and electronic properties of graphite layers grown on SiC(0001). *Surf Sci*. 2006;600(18): 3906–3911.
27. Fukidome H, Miyamoto Y, Handa H, Saito E, Suemitsu M. Epitaxial growth processes of graphene on silicon substrates. *Jpn J Appl Phys*. 2010;49(1S):01AH03.
28. Suemitsu M, Miyamoto Y, Handa H, Konno A. Graphene formation on a 3C-SiC(111) thin film grown on Si(110) substrate. *e-J Surf Sci Nanotechnol*. 2009;7:311–313.
29. Miyamoto Y, Handa H, Saito E, et al. Raman-scattering spectroscopy of epitaxial graphene formed on SiC Film on Si substrate. *e-J Surf Sci Nanotechnol*. 2009;7:107–109.
30. Huang H, Wong SL, Tin CC, et al. Epitaxial growth and characterization of graphene on free-standing polycrystalline 3C-SiC. *J Appl Phys*. 2011;110(1):014308–014305.
31. Liu F, Gutes A, Laboriante I, Carraro C, Maboudian R. Graphitization of n-type polycrystalline silicon carbide for on-chip supercapacitor application. *Appl Phys Lett*. 2011;99(11):112104–112103.
32. Echtermeyer TJ, Britnell L, Jasnos PK, et al. Strong plasmonic enhancement of photovoltage in graphene. *Nat Commun*. 2011;2:458.
33. Mueller T, Xia F, Avouris P. Graphene photodetectors for high-speed optical communications. *Nat Photon*. 2010;4(5):297–301.
34. Yang Y, Asiri AM, Tang Z, Du D, Lin Y. Graphene based materials for biomedical applications. *Mater Today*. 2013;16(10):365–373.
35. Ouerghi A, Belkhou R, Marangolo M, et al. Structural coherency of epitaxial graphene on 3C-SiC(111) epilayers on Si(111). *Appl Phys Lett*. 2010;97(16):161905–161903.
36. Ouerghi A, Marangolo M, Belkhou R, et al. Epitaxial graphene on 3C-SiC(111) pseudosubstrate: structural and electronic properties. *Phys Rev B Condens Matter Mater Phys*. 2010;82(12):125445.
37. Ouerghi A, Kahouli A, Lucot D, et al. Epitaxial graphene on cubic SiC(111)/ Si(111) substrate. *Appl Phys Lett*. 2010;96(19):191910–191913.
38. Suemitsu M, Fukidome H. Epitaxial graphene on silicon substrates. *J Phys D Appl Phys*. 2010;43(37):374012.
39. Takahashi R, Handa H, Abe S, et al. Low-energy-electron-diffraction and X-ray-photoelectron-spectroscopy studies of graphitization of 3C-SiC(111) thin film on Si(111) substrate. *Jpn J Appl Phys*. 2011;50(7):070103.
40. Aryal HR, Fujita K, Banno K, Egawa T. Epitaxial graphene on Si(111) substrate grown by annealing 3C-SiC/carbonized silicon. *Jpn J Appl Phys*. 2012;51(1S):01AH05.
41. Coletti C, Emtsev KV, Zakharov AA, Ouisse T, Chaussende D, Starke U. Large area quasi-free standing monolayer graphene on 3C-SiC(111). *Appl Phys Lett*. 2011;99(8):081904–081903.
42. Fukidome H, Abe S, Takahashi R, et al. Controls over structural and electronic properties of epitaxial graphene on silicon using surface termination of 3C-SiC(111)/Si. *Appl Phys Express*. 2011; 4(11):115104.
43. Hsia B, Ferralis N, Senesky DG, Pisano AP, Carraro C, Maboudian R. Epitaxial graphene growth on 3C–SiC(111)/AlN(0001)/Si(100). *Electrochem Solid State Lett*. 2011;14(2):K13–K15.
44. Aristov VY, Urbanik G, Kummer K, et al. Graphene synthesis on cubic SiC/Si wafers. Perspectives for mass production of graphene-based electronic devices. *Nano Lett*. 2010;10(3):992–995.
45. Portail M, Zielinski M, Chassagne T, Roy S, Nemoz M. Comparative study of the role of the nucleation stage on the final crystalline quality of (111) and (100) silicon carbide films deposited on silicon substrates. *J Appl Phys*. 2009;105(8):083505–083507.

46. Virojanadara C, Syväjarvi M, Yakimova R, Johansson LI, Zakharov AA, Balasubramanian T. Homogeneous large-area graphene layer growth on 6H-SiC(0001). *Phys Rev B Condens Matter Mater Phys*. 2008;78(24):245403.

47. Derycke V, Soukiassian P, Mayne A, Dujardin G, Gautier J. Carbon atomic chain formation on the β-SiC(100) surface by controlled sp → sp^{3} transformation. *Phys Rev Lett*. 1998;81(26):5868–5871.

48. Miller DL, Kubista KD, Rutter GM, et al. Structural analysis of multilayer graphene via atomic moiré interferometry. *Phys Rev B Condens Matter Mater Phys*. 2010;81(12):125427.

49. Chaika A, Molodtsova O, Zakharov A, et al. Continuous wafer-scale graphene on cubic-SiC(001). *Nano Res*. 2013;6(8):562–570.

50. Siegel DA, Zhou SY, El Gabaly F, Schmid AK, McCarty KF, Lanzara A. Three-fold diffraction symmetry in epitaxial graphene and the SiC substrate. *Phys Rev B Condens Matter Mater Phys*. 2009;80(24):241407.

51. Hibino H, Kageshima H, Maeda F, Nagase M, Kobayashi Y, Yamaguchi H. Microscopic thickness determination of thin graphite films formed on SiC from quantized oscillation in reflectivity of low-energy electrons. *Phys Rev B Condens Matter Mater Phys*. 2008;77(7):075413.

52. Penuelas J, Ouerghi A, Lucot D, et al. Surface morphology and characterization of thin graphene films on SiC vicinal substrate. *Phys Rev B Condens Matter Mater Phys*. 2009;79(3):033408.

53. Calizo I, Ghosh S, Bao W, Miao F, Ning Lau C, Balandin AA. Raman nanometrology of graphene: temperature and substrate effects. *Solid State Commun*. 2009;149(27–28):1132–1135.

54. Ni ZH, Chen W, Fan XF, et al. Raman spectroscopy of epitaxial graphene on a SiC substrate. *Phys Rev B Condens Matter Mater Phys*. 2008;77(11):115416.

55. Ferralis N, Maboudian R, Carraro C. Evidence of structural strain in epitaxial graphene layers on 6H-SiC(0001). *Phys Rev Lett*. 2008;101(15):156801.

56. Ferrari AC, Robertson J. Interpretation of Raman spectra of disordered and amorphous carbon. *Phys Rev B Condens Matter Mater Phys*. 2000;61(20):14095–14107.

57. Cançado LG, Takai K, Enoki T, et al. General equation for the determination of the crystallite size La of nanographite by Raman spectroscopy. *Appl Phys Lett*. 2006;88(16):163106.

58. Cançado LG, Pimenta MA, Neves BR, Dantas MS, Jorio A. Influence of the atomic structure on the Raman spectra of graphite edges. *Phys Rev Lett*. 2004;93(24):247401.

59. Sharma N, Oh D, Abernathy H, Liu M, First PN, Orlando TM. Signatures of epitaxial graphene grown on Si-terminated 6H-SiC (0001). *Surf Sci*. 2010;604(2):84–88.

60. Malard LM, Pimenta MA, Dresselhaus G, Dresselhaus MS. Raman spectroscopy in graphene. *Phys Rep*. 2009;473(5–6):51–87.

61. Maultzsch J, Reich S, Thomsen C. Double-resonant Raman scattering in graphite: interference effects, selection rules, and phonon dispersion. *Phys Rev B Condens Matter Mater Phys*. 2004;70(15):155403.

62. Röhrl J, Hundhausen M, Emtsev KV, Seyller T, Graupner R, Ley L. Raman spectra of epitaxial graphene on SiC(0001). *Appl Phys Lett*. 2008;92(20):201918.

63. Calizo I, Bejenari I, Rahman M, Liu G, Balandin AA. Ultraviolet Raman microscopy of single and multilayer graphene. *J Appl Phys*. 2009;106(4):043509.

64. Yoon D, Moon H, Cheong H, Choi J, Choi J, Park B. Variations in the Raman spectrum as a function of the number of graphene layers. *J Korean Phys Soc*. 2009;55(3):1299–1303.

65. Dresselhaus MS, Dresselhaus G, Saito R, Jorio A. Raman spectroscopy of carbon nanotubes. *Phys Rep*. 2005;409(2):47–99.

66. Ferrari AC, Meyer JC, Scardaci V, et al. Raman spectrum of graphene and graphene layers. *Phys Rev Lett*. 2006;97(18):187401.

67. Pimenta MA, Dresselhaus G, Dresselhaus MS, Cançado LG, Jorio A, Saito R. Studying disorder in graphite-based systems by Raman spectroscopy. *Phys Chem Chem Phys*. 2007;9(11):1276–1290.

68. Ushio S, Yoshii A, Tamai N, Ohtani N, Kaneko T. Epitaxial graphene growth on 4H-SiC (0001) with precisely controlled step-terrace surface by high temperature annealing above 2000°C in UHV. *Phys Status Solidi*. 2011;8(2):580–582.

69. Sprinkle M, Hicks J, Tejeda A, et al. Multilayer epitaxial graphene grown on the SiC(000-1) surface; structure and electronic properties. *J Phys D Appl Phys*. 2010;43(37):374006.

70. Cong C, Yu T, Wang H. Raman study on the G mode of graphene for determination of edge orientation. *ACS Nano*. 2010;4(6):3175–3180.

71. Casiraghi C, Hartschuh A, Qian H, et al. Raman spectroscopy of graphene edges. *Nano Lett*. 2009;9(4):1433–1441.

72. Ben Gouider Trabelsi A, Ouerghi A, Kusmartseva OE, Kusmartsev FV, Oueslati M. Raman spectroscopy of four epitaxial graphene layers: macro-island grown on 4H-SiC substrate and an associated strain distribution. *Thin Solid Films*. 2013;539:377–383.

73. Rosenwaks Y, Shikler R, Glatzel T, Sadewasser S. Kelvin probe force microscopy of semiconductor surface defects. *Phys Rev B Condens Matter Mater Phys*. 2004;70(8):085320.

74. Yu YJ, Zhao Y, Ryu S, Brus LE, Kim KS, Kim P. Tuning the graphene work function by electric field effect. *Nano Lett*. 2009;9(10):3430–3434.

75. Filleter T, Emtsev KV, Seyller T, Bennewitz R. Local work function measurements of epitaxial graphene. *Appl Phys Lett*. 2008;93(13):133117.

76. Hibino H, Kageshima H, Kotsugi M, Maeda F, Guo FZ, Watanabe Y. Dependence of electronic properties of epitaxial few-layer graphene on the number of layers investigated by photoelectron emission microscopy. *Phys Rev B Condens Matter Mater Phys*. 2009;79(12):125437.

77. Datta SS, Strachan DR, Mele EJ, Johnson AT. Surface potentials and layer charge distributions in few-layer graphene films. *Nano Lett*. 2008;9(1):7–11.

78. Silly MG, Roy J, Enriquez H, et al. Initial oxide/SiC interface formation on C-terminated β-SiC(100) c(2 × 2) and graphitic C-rich β-SiC(100) 1 × 1 surfaces. *J Vac Sci Technol B Microelectron Nanometer Struct Process Meas Phenom*. 2004;22(4):2226–2232.

79. Sljivančanin Z, Andersen M, Hornekær L, Hammer B. Structure and stability of small H clusters on graphene. *Phys Rev B Condens Matter Mater Phys*. 2011;83(20):205426.

80. Emtsev KV, Speck F, Seyller T, Ley L, Riley JD. Interaction, growth, and ordering of epitaxial graphene on SiC{0001} surfaces: a comparative photoelectron spectroscopy study. *Phys Rev B Condens Matter Mater Phys*. 2008;77(15):155303.

81. Starke U, Riedl C. Epitaxial graphene on SiC(0001) and SiC(000-1): from surface reconstructions to carbon electronics. *J Phys Condens Matter*. 2009;21(13):134016.